Keywords
stroke detection, brain image segmentation, multi-classification, MRI brain image, bio-inspired deep learning

Authors
R.Punitha Lakshmi[1]
Department of ECE, Puducherry Technological University. Puducherry, India. Email: punitha278@ptuniv.edu.in

V.Vijayalakshmi[2]
Department of ECE, Puducherry Technological University, Puducherry, India. Email: vvijizai@ptuniv.edu.in

Received:19-06-2026
Revised:23-07-2026
Accepted: 04-08-2026
Doi:10.1922/ejprd.v34i7s.1678

Segmentation of Brain Stroke MRI Images by Bio Inspired Genetic Swarm Clonal Algorithm and Multi-Classification of Stroke using Deep Adversarial Naïve Segnet Architecture

Abstract
Human stroke incidence has been progressively rising recently for a variety of reasons. The patient's management depends critically on the type of brain stroke that has been diagnosed. Although magnetic resonance imaging (MRI) is a commonly utilized diagnostic method for stroke, manual interpretation of MRI results by professionals is laborious and time-consuming. For automatic segmentation as well as categorisation of stroke on brain MRI, computer-aided diagnostic (CAD) models are therefore required. This research proposes novel technique in stroke detection based on brain image segmentation with multi-classification in stroke detection using MRI brain image by bio-inspired deep learning model. Here the input is collected as MRI brain image in which the images have been pre-processed for noise removal and normalization. Then the processed image is segmented using conventional Boltzmann transfer convolution with genetic swarm clonal algorithm (CBTC-GSwClA). The segmented image shows the brain MRI regions with stroke prediction and the image will be classified using deep adversarial naïve SegNet architecture (DANSegNet). This classified output shows various classes of stroke ranging from stage 0 to 6. The experimental analysis has been carried out for various stages of stroke in terms of Training accuracy, Validation accuracy, Recall, Precision, F1-score, Kappa coefficient, ROC. Proposed technique achieved 96% Precision, 99% Validation accuracy, 98% Training accuracy, and a 97% F1-score, recall of 98%, kappa co-efficient of 94%.

1. Introduction

Among adult survivors globally, stroke is primary cause of death as well as disability. Hemorrhagic or ischaemic strokes are both possible. Stroke sufferers and their family bear significant physical, social, emotional, and financial costs. Approximately 15 million individuals worldwide suffer from brain strokes each year; of them, one-third pass away and the remainder are left permanently incapacitated, according to the WHO. Stroke prevalence in India ranges from 45 to 487 per 100,000 people in urban areas and from 55 to 388 per 100,000 people in rural areas. High blood pressure is mostly to blame for stroke [1]. Smoking and leading an unhealthy lifestyle are two other risk factors that contribute. By successfully managing risk factors like tobacco use, hypertension, and hyperlipidaemia, stroke incidence and mortality can be avoided. As a result, between 1990 and 2010, the incidence of stroke declined by about 10% in wealthy nations. Unfortunately, the benefit of prevention is less pronounced in poorer nations, where the incidence has increased by 10% during the same time period [2]. Hemorrhagic and ischaemic strokes can be distinguished based on their pathophysiology. About 70% of stroke cases are ischaemic in origin, characterised by neurological dysfunction that either lasts longer than 24 hours or is terminated by death within that time. Hemorrhagic strokes account for about 12% of all stroke cases; they include 3% subarachnoid and 9% intracerebral haemorrhages [3]. Hemorrhagic strokes are more likely to result in death than permanent disability because they are caused by cerebral blood vessel rupture or vascular abnormalities that leak into nearby brain regions, impairing their ability to function. Manually marking an MRI image of a single severe lesion with a convoluted shape may take many hours. To treat more patients in less time, a faster, more precise, and automatic characteristics extraction and disease detection system is necessary. Through deep learning, a computer system could be trained to perform categorisation tasks directly from photos, text, or voice. Stroke takes a terrible toll on people; each year, it causes over 5 million fatalities and 5 million permanent disabilities. Of all strokes, 20% are classified as intracerebral hemorrhagic strokes (ICH), with ischaemic strokes (IS) making up the majority of cases. At the moment, stroke is diagnosed using Computed Tomography (CT) as well as MRI. Treatment is currently available for a tiny proportion of patients (between 1% and 8%), mostly because of lengthy travel time. The goal of ongoing efforts is to streamline diagnosis processes in order to create a small system that can differentiate between hemorrhagic and ischaemic strokes in a pre-hospital setting. Due to its facile penetration through skull, microwave propagation in human tissue is currently the subject of research efforts. Using microwave frequencies, medical microwave imaging is a non-invasive medical imaging method that produces images of the body's internal tissues [4]. In some situations, deep learning systems may be able to achieve accuracy levels that exceed those of humans. Large amounts of data sets and multilayer neural network components are used to train models. Using a technology called deep learning, an automated intelligent system can mimic human learning. Predictive modelling and statistics are part of data science, which also includes deep learning. Data researchers, who are in charge of gathering, evaluating, and interpreting vast amounts of data, will find it to be of great use. Deep Learning expedites and simplifies the process. It is a prominent area of study with numerous applications. To classify images, convolutional neural networks, or CNNs, are employed [5]. At its most basic, deep learning may be thought of as a way to automate data analytics. DL algorithms, in contrast to conventional ML algorithms, are developed in a hierarchy of progressively greater difficulty. Numerous medical imaging modalities are used, including PET, MRI, CT. Additionally, some compounds can be seen at concentrations too low to impact contrast of conventional MR imaging and too low to be directly recognised in MRS at standard water imaging resolution thanks to a special MR technique termed chemical exchange saturation transfer (CEST). Among these, an MRI scan uses microwave pulses and magnetisation to provide a non-invasive image of the inside anatomy of the body. Three types of T1 weighted, T2 weighted, Fluid Attenuated Inversion Recovery (FLAIR) MRI patterns are used to diagnose brain strokes. Challenge of using brain MRI to identify and detect stroke-infected regions is critical [6].

2. Research contribution:

- To suggest a novel method for detecting strokes using MRI brain images that combines multi-classification with brain image segmentation.
- The input is an MRI brain image that has been pre-processed for normalisation and noise reduction. Following processing, the picture is segmented using the conventional Boltzmann transfer convolution with genetic swarm clonal algorithm (CBTC-GSwClA).
- After the picture has been segmented, deep adversarial naïve SegNet architecture (DANSegNet) will be used to classify the image, which displays the brain MRI areas with stroke prediction.

3. Related works:

Deep learning technology has advanced quickly over the last few decades and has many uses in the medical industry. CNN has been used specifically for lesion detection, showing a 13–34% increase in accuracy. A spatially restricted convolutional neural network (SC-CNN) was employed in study [7] to identify and categorise colorectal cancer cells. In place of more conventional feature classification techniques, it uses the neighbouring ensemble predictor (NEP) technique for recognition as well as classification, which has the potential to reach greater accuracy. Author [8] employed 3D CNN, which can extract more representative advanced characteristics, to automatically diagnose cerebral haemorrhage (CMBS) from MR images. When comparing 3D CNN detection accuracy to 2D CNN as conventional manual feature extraction, it can reach up to 93.16%. Numerous CNN architectures have shown remarkable success in identifying a wide range of illnesses. As a result, the field of medicine offers a lot of opportunities quick development of DL. Lesion detection in medical photos is a significant use of deep learning. Deep learning has the potential to increase medical

diagnosis accuracy and timeliness by efficiently extracting valuable information from training data. In work [9], stroke incidence was predicted using C4.5 decision tree techniques as well as k-nearest neighbour methods. The results showed that the C4.5 decision tree techniques produced a higher accuracy rate of 95.42%. Another group [10] demonstrated that SVM was more accurate in predicting the outcome of stroke thrombolysis when they combined it with machine learning techniques. Work [11] used two ANN methods with accuracy values of 79.2% and 95.1% to predict ischaemic stroke. A study [12] predicted the presence of stroke using knowledge discovery process. According to the study's findings, ANN performed better than other methods in terms of prognosis. In order to classify ischaemic stroke, author [13] used nine classification techniques, such as generalised linear methods, random decision forests (RDFs), convolutional neural networks (CNNs). RDFs and CNNs, in particular, offer higher classification accuracy than the other techniques. In order to predict stroke, work [14] employed decision trees (DTs), naive Bayes, ANN. It was found that DT produced a better categorisation than the other approaches. Author [15] showed that kNN has superior accuracy over other models by predicting stroke severity index (SSI) using kNN, regression tree model, and multiple linear regression (MLR). Work [16] provided a dataset of electronic medical claims so that the efficacy of DNN with ML methods for stroke detection could be compared. When compared to other machine learning algorithms, DNN and RF techniques have proven to perform better. Author [17] devised a hybrid machine learning technique for stroke prediction. To find missing data, Radom Forest regression is first applied. Second, DNN is used for autonomous hyperparameter optimization for stroke diagnosis. A feed forward neural network with back propagation was employed in a study [18] to diagnose stroke by predicting cerebral ischaemia, one of the risk factors for stroke. A novel approach for using EEG signals to diagnose stroke was described by author [19]. They combined fuzzy entropy, wavelet packet energy, hierarchical theory to work on a multi-feature fusion. The fusion method produced better outcomes when it came to diagnosing ischaemic and hemorrhagic strokes. A comprehensive method for evaluating the degree of an ischemic stroke from a radiography text using ML as well as NLP was presented in a study [20]. The author [21] introduced two deep learning models for MRI image diagnostics for stroke prediction: LeNet and SegNet. 96% classification accuracy and 85% segmentation accuracy were attained with the SegNet model. The Xception model was created by Work [22] to diagnose a middle cerebral artery indication on CT scans. Methods results showed 86.5% accuracy, 82.9% sensitivity, and 89.7% specificity. The author [23] employed deep learning technology to estimate the risk of stroke using a dataset on heart illness. The findings demonstrated that, in comparison to the error prior to calibration, the error rate is lower and the calibration gain is almost equal to 1. In order to determine the risk of osteoporosis in postmenopausal women, work [24] developed and validated a number of ML methods, RF, ANN, LR. Cited authors used medical records from Korean National Health and Nutrition Surveys. Only comparatively small datasets were used, despite the fact that its accuracy was adequate [25]. The research paper is structured as follows: Section 1 gives the introduction for stroke, research contributions are listed in Section 2, detailed literature survey is explained in Section 3, Existing segmentation works are explained in Section 4, Proposed stroke detection segmentation techniques are explained in Section 5 & 6 classification model is given in Section 7, followed by the results and future scope in Section 8.

4. Stroke Background:

Cerebrovascular diseases are defined as brain disorders that result from congenital or acquired blood vessel injury, hemorrhagic or ischaemic causes (ischaemic stroke), or both. The effects might be temporary or permanent. The middle-aged and elderly are the groups most affected by these disorders. One of the causes of stroke is ischaemic cardiovascular disease (CVD); hence, one of the ways to prevent one of the causes of stroke is by early detection of CVD disorders by family members as well as consultation with specialists to receive appropriate treatment. An examination of the airway and circulation should be part of the first assessment. Brain hemorrhagic episodes can be brought on by a prior injury. They are caused by rupture of a cerebral artery inside parenchymal tissue. Stroke often happens in an instant, with symptoms including headache, dizziness, nausea, localised neurological impairments depending on where the brain haemorrhage originates. After the physician has determined that the patient is suffering from a stroke that is affecting a particular vascular region in brain as well as resulting in a particular neurological deficit, next step is to determine if cerebral hemorrhage is hemorrhagic or ischemic in nature. An MRI or CT scan is necessary for this condition. Treatment for hemorrhagic stroke involves managing bleeding as well as lowering pressure with drugs or an expeditious surgical procedure, should imaging confirm the condition. Location of bleeding as well as whether it has happened inside or outside of brain tissue determine kind of treatment that is needed.

5. Proposed stroke detection segmentation and classification model:

As Figure 1 shows the proposed model is comprised of segmentation and classification model blocks, which make up the proposed classifier for multi-classification. Two stages are used in the construction and assessment of the classifier: (1) a training phase and (2) a testing phase. The classifier is trained using randomly chosen photos from the datasets during the training phase. The classifier can classify the query photos once it has been trained.

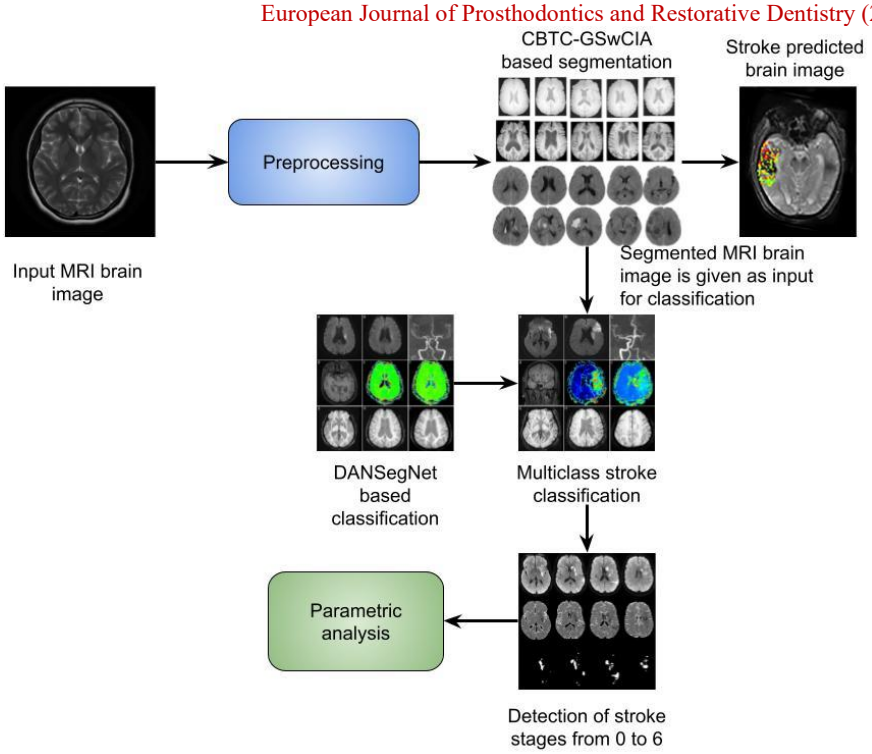

Figure-1 Proposed stroke detection model

Data pre-processing: A sequence of 3D images was stacked and shrunk as a 2D array. Preprocessing images is important for analysing medical images. Techniques for picture augmentation and denoising are employed to maintain image quality. The resulting noise was eliminated by using a median filter. Every pixel value was substituted with the median of its neighbours, and those that differed significantly from their neighbours were removed. Next, rescale the pixel range between 0 and 1 to conduct normalisation on the data. Next, extract the minimum and maximum values from the images. Finally, convert the N-dimensional image into a new intensity value in range New= {new_min...new_max}. Equation (1) provides calculation for the normalisation.

$$I(new) = \frac{I - I(min)}{I(max) - I(min)} \qquad (1)$$

Patient's position inside scanner, his motions, other elements that cause variations in the MRI pictures' brightness are some of the factors that impact the quality of the images. The bias field is the difference between the black and white MRI intensity values. Negative, slick, or undesired signals can ruin an MRI picture. All processing algorithms will produce inaccurate results if the bias field is not corrected. In order to achieve consistent accuracy in the subsequent stages, the preprocessing algorithms eliminate the noise and fix the bias field-related errors. Image quality enhancement pre-processing methods piqued the interest of researchers. In this work, the image was scaled for colour constancy and the mean RGB colour for MRI scans was found. Lastly, an average filter was applied to improve the MRI pictures. Every MRI picture was scaled based on the deep learning models.

6. Conventional Boltzmann transfer convolution with genetic swarm clonal algorithm (CBTC-GSwCIA):

A generative stochastic artificial neural network structure, the Boltzmann Machine is an unsupervised two-layered bipartite graph that can learn probability distributions over the inputs without supervision. The components of an RBM consist of a weight matrix W, which indicates bidirectional links between visible and hidden layers, a set of visible units (x), and a set of hidden units (y). The neurones in the visible layer of the bipartite network are tightly connected to those in hidden layers, but they remain totally isolated within same layer. concepts of DBN with consideration for the Restricted Boltzmann Machine (RBM) basis, which serves as DBN's motivation. Four RBM layers were employed by the DBN in our study to extract features. Stochastic neural networks based on energy are essentially constrained Boltzmann machines made up of two layers of neurones: visible and hidden nodes. The learning stage is guided by an unsupervised greedy design. The RBM structure consists of a visible layer (vl) with n nodes and a hidden layer (hl) with m nodes. Weight between visible node (vli) and hidden node (hlj) is represented by the matrix n × m in M. If vl and hl are the binary and hidden units, respectively, then vl ∈ {0, 1}n and hl ∈ {0, 1}m. RBM's energy function can be found by eqn (2)

$$E(vl, hl) = -\left(\sum_{i=1}^{n} c_i vl_i + \sum_{j=1}^{m} d_j hl_j + \sum_{i=1}^{n}\sum_{j=1}^{m} vl_i hl_j M_{ij}\right)$$

$$P(vl, hl) = \frac{e^{-E(vl,hl)}}{\sum_{vl,hl} e^{-E(vl,hl)}} \qquad (2)$$

Here the denominator $\sum_{vl,hl} e^{-E(vl,hl)}$ remains for all conceivable confguration of vl and hl that is a standardization factor. In this work, the image was scaled for color constancy and the mean RGB color for MRI scans was found. Lastly, an average filter was applied to improve the MRI pictures. Every MRI picture was scaled based on the deep learning models by eqn (3)

$$P(vl) = \frac{\sum_{vl} e^{-E(vl,hl)}}{\sum_{vl,hl} e^{-E(vl,hl)}} \quad (3)$$

The stochastic gradient smell algorithm calculates the logarithmic derivatives P(vl) for the parameters c, d, and M before requesting the necessary conditions.

A multi-phase training procedure was employed by our models. In order to identify strokes, the brain halves were fed into the model individually in the first phase. If a picture showed a stroke lesion, the brain halves were labelled as positive (1). For this assignment, 2D model was trained from scratch. For faster convergence, we built initial weights for our 3D model in a self-supervised manner prior to stroke side identification job. Following training, first 2 convolutional layers/blocks were frozen in the model. Only photos with stroke lesions were used as input in a subsequent training phase, which made use of this pretrained network. To create a single, slice-level output, attention model as well as convolutional outputs were concatenated into a feature vector and fed into a fully-connected layer. We were able to create an image-level prediction by combining these slice-level forecasts in this way. Attention model as well as trainable weight factor, which assign pixel-level and slice-level relevance that are learned and optimized, allow method to localize to salient regions.

In transfer learning, a domain is described as D={X,P(X)}, where P(X) is a marginal probability distribution with X={x1,…,xn}⊂X and X is the feature space. For example, P(X) may depend on subject groups like teenagers or the elderly, and X may comprise all conceivable images obtained from a specific MRI protocol, acquisition parameters, scanner hardware. Tasks consist of a decision function f and a label space Y, or T={Y,f}. It is necessary to learn decision function from training set of data (X,Y). For instance, predicting the survival rate of stroke patients is one of the tasks performed during MR brain imaging. It is crucial that TS and DS have a relationship with TT and DT, respectively, as transfer learning may deteriorate accuracy on the target domain otherwise.

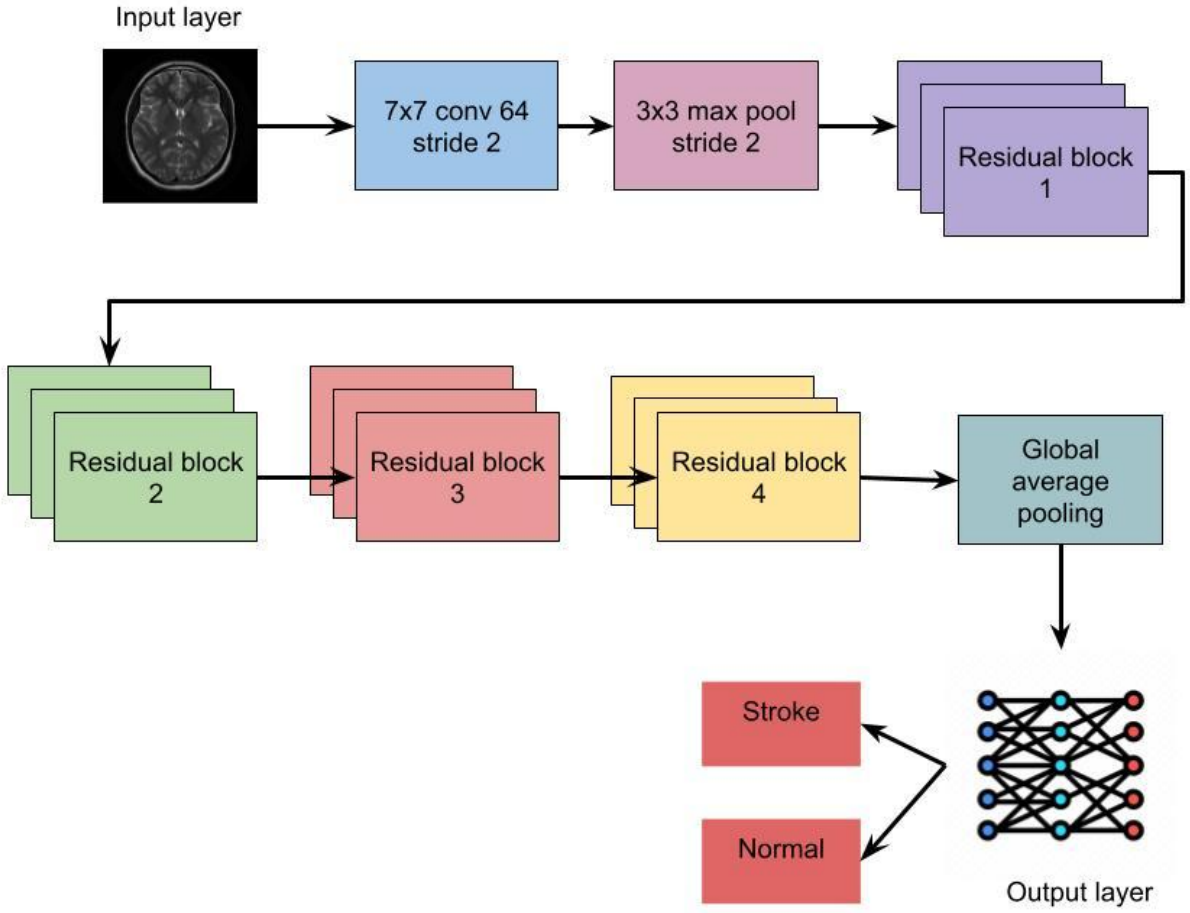

Figure-2 proposed transfer convolutional architecture

The stacked layers in ResNet are trained to fit a residual map. Three convolutional layers make up the residual function F(x) in ResNet-50: a layer with 1 × 1 filters, a layer with 3 × 3 filters, and a layer with 1 × 1 filters. Batch normalisation (BN), which employs rectified linear units (ReLU) as activation function, comes after each of aforementioned layers. Lastly, element-wise addition is carried out between the shortcut connection (x) and the stacked layers' output (F(x)). After that, a different ReLU activation function receives the sum. Identity mapping is carried out by shortcut connections between Residual Blocks 1, 2, 3, and 4. When the shortcut crosses feature

maps of two sizes, the dotted boundary residual blocks in Figure 2 are utilised to raise the dimensions with a stride of 2, and a projection shortcut is employed to match the dimensions. Next, the input is convolved using 64 7 × 7 kernels at a stride of 2, and then it is max pooled at a stride of 2. To compress the output feature map to 1 × 1 × 2048, the output is then fed to a sequence of stacked residual blocks and then subjected to global average pooling (GAP). A fully linked layer of 64 neurones classifies these 2048 attributes, and an output layer with a sigmoid activation function comes next. The input brain MRI image is classified as stroke if the output sigmoid neuron is greater than 0.5; otherwise, it is classified as non-stroke (normal).

In order to configure GA, the problem's solution must be encoded as chromosomes, and the chromosomes' fitness must be calculated. We use a single bit of 1/0 in a chromosomal space to encode each feature xi in the feature space X = [x1, x2, • • •, xn] in our GA configuration. The bit 1/0 indicates that the ith feature is either selected or not selected, accordingly. To represent the chromosomes (the positions of the STROKEs) in terms of bits, we decided to employ a binary encoding technique (0s and 1s). When used in optimisation issues, binary encodings can offer a number of benefits, including the ability to easily alter individual bits within the representation. One of the main advantages of a binary encoding for our problem is that it makes it possible to efficiently represent numerous variables within a single chromosome. In particular, this method allows for the depiction of number of bits (i.e., prospective sites) and number of STROKEs (i.e., 1s) that are present on the same chromosome. By employing a fixed-length chromosome, where every bit represents a possible location for a STROKE, this encoding streamline representation of solution. Additionally, it offers a standardised method for applying genetic operators to the chromosome during the optimisation process, such as crossover as well as mutation. Every chromosome has three STROKEs, each of which is encoded with 39 bits, similar to the case of the three STROKEs settings. In light of the STROKE locations, we thereby activate three bits, for instance, (1, 2, 5) → (11001000000000000000000000000000000000). Proposed model is capable of efficiently manipulating the representation and implementing crossover and mutation procedures more quickly because of the binary encoding, which eliminates the need for any operations to be performed in the succeeding steps.

A population of GA chromosomes uses mutations as a genetic operator to preserve genetic variation from generation to generation. The objective is to increase variety of the population by arbitrarily altering one chromosome by a small amount (corresponding to a place). In order to do this, we employ a hyper-parameter called mutation rate, which establishes likelihood that a mutation will take place in a STROKE position, or a single chromosomal bit. The inclusive range of the mutation rate is 0 to 1. A chromosome can be mutated by going through each STROKE site (bit) among the I possible locations (bits) as well as flipping it (from 0 → 1 or 1 → 0) according to the mutation rate in order to produce the desired result. A decent mutation rate is often recommended to be 1/L, where L is the bitstring's length (or, in this case, the total number of possible sites). Positions of each "1" bit in input string are determined, mutation rate per "1" bit is computed, as part of our specified mutation strategy. As soon as we have "flipped" one bit, this process ends. Every "1" bit is assessed separately, event of a mutation, the procedure guarantees that the total number of "1" bits in string doesn't change. Since shuffle crossover operator lets us regulate number of 1s in a bit string that represents stroke placements, we discovered that it closely matches our situation. We created a crossover operator based on shuffle crossover, which involves utilizing mathematical set operations to rearrange bits between two parental chromosomes.

Swarm clonal algorithm (SCA):

The SCA is a populated global optimization technique that was inspired by studies of fish schools and flocking behaviour's in the air. The implementation is quick and simple. In addition, we included cross-validation in the construction of the fitness function for SCA. Search is carried out by SCA using a swarm of particles that are updated every iteration. Each particle searches for the optimum solution by moving in the following directions: toward its previous best position (pbest) and toward the best global location in the swarm (gbest) by eqn (4)

$$p_{best_i} = p_i(k^*)$$
$$\text{s.t. fitness}\left(p_i(k^*)\right) = \min_{k=1,\ldots,t}\left[\text{fitness}\left(p_i(k)\right)\right]$$
$$g_{best} = p_i(k^*)$$
$$\text{s.t. fitness}\left(p_{i^*}(k^*)\right) = \min_{i=1,\ldots,P}\left[\text{fitness}\left(p_i(k)\right)\right] k = 1, \ldots, t \quad (4)$$

where P is total number of particles, t is number of iterations that are currently in progress, k is iteration index, i is particle index. Following equations can be used to update particle position and velocity by eqn (5)

$$v_i(t+1) = wv_i(t) + c_1 r_1\left(p_{best_j}(t) - p_i(t)\right) + c_2 r_2\left(g_{best}(t) - p_i(t)\right)$$
$$p_i(t+1) = p_i(t) + v_i(t+1), \quad (5)$$

where v stands for speed. Worldwide exploration and local exploitation are balanced by inertia weight w. Within range of (0, 1), random variables r1 and r2 have a uniform distribution. "Acceleration coefficients" are the positive constant parameters c1 and c2. In this case, the parameters C and σ in (13), together form the particle encoding.

Cross-Validation

Taking into account the optimal trade-off between computational cost and accurate estimations, we select five. Five mutually exclusive subsets of roughly equal size are randomly selected from the dataset; four of these subsets are utilized as training sets, remaining subset is utilized as validation. Every subset is utilized once for validation because the aforementioned process is done five times. The 5-fold cross-validation classification accuracy was selected by the PSO fitness function as follows by eqn (6)

$$\text{fitness} = \frac{1}{5}\sum_{i=1}^{5}\left|\frac{y_s}{y_s + y_m}\right| \quad (6)$$

Here, the numbers for successful and incorrect classifications are indicated by ys and ym, respectively.

PSO is used to maximize classification accuracy, or the fitness function. The following optimization issue is solved by the algorithm using the clonal selection concept by eqn (7)

$$x^* = \arg\max_{x \in R^0} f(x)$$
$$N_c = \sum_{i=1}^{n} n_i = \alpha^* n, \quad (7)$$

with α, the clonal multiplication factor that determines the cloning number by taking a positive integer. For every antibody used in this paper, ni is the same and equals α in order to find many optima and arrive at the global optimum. Three phases are involved in applying hypermutation to each chosen antibody Abk I and its clones in Ck. First, as follows, a transient antibody is produced by eqn (8)

$$Z = \frac{\left(Ab_d^k + Ab_i^k\right)}{2} + F \cdot \left[\left(Ab_d^k - Ab_i^k\right) + \left(Ab_s^k - Ab_c^k\right)\right] \quad (8)$$

$f\left(Ab_d^k\right) \leq f\left(Ab_i^k\right)$, Ab_b^k and Ab_c^k are also randomly selected from Ck, with F a user-specified scaling factor, and Abk d randomly selected from Ck such that f(Ab_d^k)≤f(Ab_i^k). Subsequently, every temporary antibody Z and its parent Abk i undergo the following crossover to produce a trial antibody Ab*k I by eqn (9)

$$Ab_{L,j}^* = \begin{cases} Z_j & \text{if } (\text{rand} < CR) \\ Ab_{i,j}^k & \text{otherwise} \end{cases}, j = 1, \cdots, D \quad (9)$$

with the user-specified crossover rate (CR) and a uniformly distributed random number (rand) falling between [0, 1]. If obtained trial antibody Ab*k i has a better affinity than original antibody Abk i, it substitutes Abk i in Ck during the combination stage; if not, Abk i is retained.

Algorithm of CBTC-GSwClA
Input: observed brain MR image Y
Output: optimal voxel class labels X and method parameters θ.
Start: segmentation by CBTC, random method parameters and initial bias field b
while stopping criterion is not met
Calculate vector f^k through Eq. (11)
Choose $Ab_{(n)}^k$
Choose $Ab_{(M)}^k$
Clone $Ab_{(m)}^k \rightarrow C^k$
Hypermutation using DE $C^k \rightarrow C^{*k}$
Reselect from C^{tk} to partly replace Ab^k
$Ab_{(d)}^k$ replace the d lowest affinity from Ab^k using EDA
Update class labels in Eq. (9) using the SCA algorithm
Update bias field utilizing technique
end
Evaluate step 2 to 12 again with ranges of θ

7. Deep adversarial naïve SegNet architecture (DANSegNet):

We employ a deep generative neural network architecture for the form network, which is an adaptation of the CNN GAN design used at super-resolution. In order to overcome hardware constraints on our training batch size and learn instance-specific mean as well as covariance shift, we choose to use Instance Normalisation for the discriminator instead of Batch Normalisation. A 1 × 1 convolutional block replaces the final layer, which is then followed by two dense layers and leaky ReLU. Discriminator produces a scalar judgement. In order to improve generator's capacity to learn higher levels of abstraction, we have added residual connections to 5 deconvolutional layers and a total of 6 deconvolutional layers for up-sampling. The normalisation and nonlinear activation layers are chosen to be Instance Normalisation and Exponential Linear Unit (ELU) activation function. Latter promotes natural gradients, which quickens learning. A regularly distributed latent vector of size 100 with zero mean and unit variance is fed into the generator, which outputs a 256 × 256 × 256 × 3 deformation field by eqn (10)

$$S(x) = \alpha\left(\frac{1}{1-e^{-x}} - \frac{1}{2}\right) \quad (10)$$

Equations (10) and (11), respectively, represent the cost functions that were utilised for the discriminator and generator. Here, D(x) represents decision output of discriminator given an image x, while G(z) represents image that synthesises given a random latent vector z. The regularisation coefficient for the gradient penalty, λ1, number of discriminator-per-generator updates, k, default values from paper were used by eqn (11)

$$\hat{P}(Y = k \mid X_1, \ldots, X_P) = \frac{\pi(Y=k)\prod_{j=1}^{P} P(X_j|Y=k)}{\sum_{k=1}^{K} \pi(Y=k)\prod_{j=1}^{P} P(X_j|Y=k)} \quad (11)$$

When used for classification tasks where assumptions are not met, such classifying fMRI responses elicited by various task conditions, naïve bayes classifiers frequently outperform other, more complex classifiers. To avoid having excessively redundant information in our predictor variables, we separated the modelling of aberrant and missing tissue while creating feature maps (predictors). Conditional probability of an event A, given that another event B has occurred, is provided by Bayes theorem. Issue with Naïve Bayes model is that basing such a method on probability tables is impractical if number of characteristics (n) is huge. As a result, we rewrite the model to make it easier to understand.

A downsampling (encoding) path, an equivalent upsampling (decoding) path, and a final pixelwise classification layer make up the SegNet architecture. Thirteen convolutional layers in the encoder path correspond to initial thirteen convolutional layers in VGG16 network. Since every encoder layer has an equivalent decoder layer, there are 13 convolutional layers in decoder network as well. Initial two convolution blocks have two layers each, whereas the latter three blocks have three layers each. Decoder path is structurally identical to encoder path, with the exception that an upsampling operation has taken the place of the max-pooling operation. Outputs of preceding layer and output of matching encoding layer's max pooling indices are utilized as input for upsampling. A soft-max classifier layer receives high dimensional feature representation produced by the final decoder and classifies every pixel independently.

For the purpose of segmenting brain strokes from multi-modal MR data, SegNet models are customised and trained independently. While the deeper layers of the SegNet models learn more intricate and practical finer features, the initial levels only learn basic features like edges and circles. Each SegNet model's final deconvolution layer contains machine-learned features that correspond to four score maps: background, necrosis, oedema, and augmenting stroke. From the 16 feature maps that were obtained, the four top scoring maps are created. A feature vector is created using a mix of four top score maps and pixel intensity values of original MRI models in order to add even more data for categorisation. Ultimately, each voxel in the MRI picture is classified into stroke and stroke portions by applying encoded feature vector to a DT classifier. The last layer in architecture, called Softmax layer, uses feature maps that last level of decoder returned to return prediction probabilities of input MRI pictures in desired format (240x240x7). Given that segmentation task at hand is actually a multiclass classification problem with seven outputs (classes) as outcomes.

8. Results and discussion:

Hardware configuration: An Intel(R) Xeon(R) CPU E5-2680 v2 @2.80GHz, two Nvidia TESLA P-100 graphics cards with 16 GB dedicated memory, and 187 Gb of RAM were used in the experiments. The platform was GPU-based and high-performance computing. During the training phase, the average compute time for an epoch is 2.03 seconds, with a batch size of 64 samples. An Intel Xeon E5-2650 V4 processor with 128 GB of total memory and a high-performance GPU (NVIDIA Tesla P40) with 3840 CUDA cores were used for the MRI pretreatment on a Think Server TS560 running Linux (Ubuntu 16.10). Python 2.7.12 was used to implement all of the techniques. Using TensorFlow-based deep learning, NN is constructed utilizing Keras package. When analysing imaging data, analysts were blinded to the identities of all subjects. When Keras library is used, the optimal model can be automatically saved. The system specs employed in this experiment are listed in Table 1.

Table 1 Computational System Specification used for experimentation.

Component	Specification
Processor	Core i5
SSD	1 TB
RAM	11GB
GPU	NVIDIA Geforce RTS 2080 Ti
Operating system	Windows 10 pro
Development language	Python
Development tools	Pycharm community edition 2020

dataset description: The ATLAS (Anatomical Tracings of Lesions after Stroke) website, which is mostly used for neuroimaging investigations, is where the brain stroke data were found. Downloading the brain stroke dataset was possible upon acceptance of the terms and conditions. The collection included manually segmented lesions and anatomical brain scans from stroke victims. About 229 T1-weighted MRI scans with manual segmentation as well as metadata in.csv format were included in the Nifti format data, while the 400 MRI scans in the normal patient dataset were contained in the dataset. We employed a batch size of 50 and trained method across 200 epochs. With suggested optimiser and binary cross entropy loss function, experiment's learning rate is set at 0.001.

9. Proposed model analysis:

Table-2 Processing of input MRI brain image using proposed segmentation and classification techniques

Input MRI image	Pre-processed image	Segmented image	Classified image	Stage of stroke

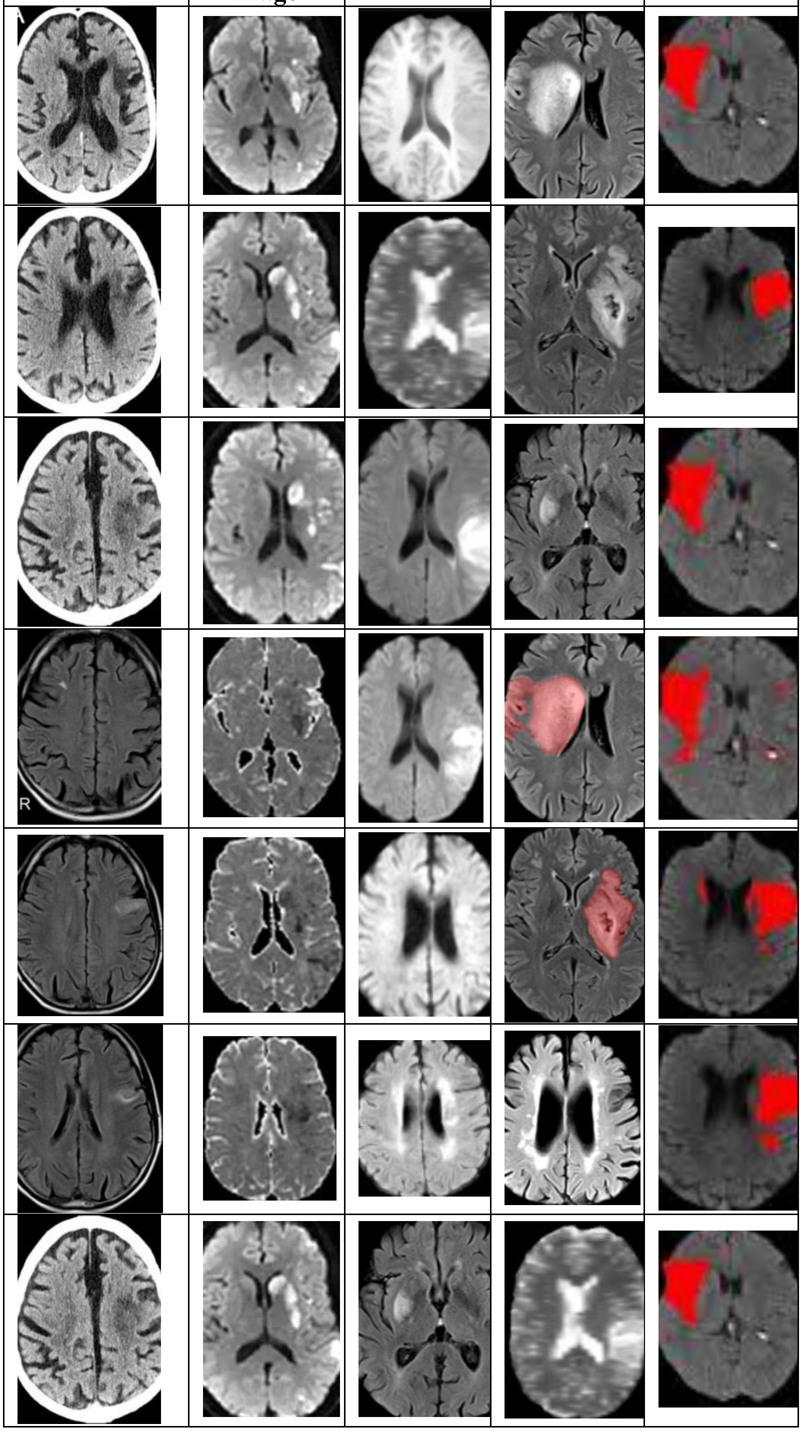

The processing of different input MRI image datasets for stroke detection is displayed in Table 2 above. Here, segmented characteristics from the processed brain MRI image at different phases as well as the output that has been classed are displayed. Figure 3 illustrates the common use of a confusion matrix in determining these performance measures. Both the expected and actual categories are represented in this matrix. A confusion matrix is commonly utilized to evaluate these performance parameters (see fig. 3). The actual and predicted classes are both covered by this matrix. Number of positive classifications that are correctly classified as positive is represented by True Positive (TP) values; number of negative classifications that are correctly classified as negative is represented by True Negative (TN) values; number of negative classifications that are incorrectly classified as positive is represented by False Positive (FP) values; number of positive classifications that are incorrectly classified as negative is represented by False Negative (FN) values. One technique for assessing how well ML categorisation algorithms perform is the confusion matrix. Every model that has been developed has had its effectiveness evaluated using confusion matrix. Confusion matrix shows the frequency of accurate

forecasting and inaccurate estimation by our models. While true positives and true negatives were given to appropriately anticipated values, FP and FN were assigned to poorly projected values.

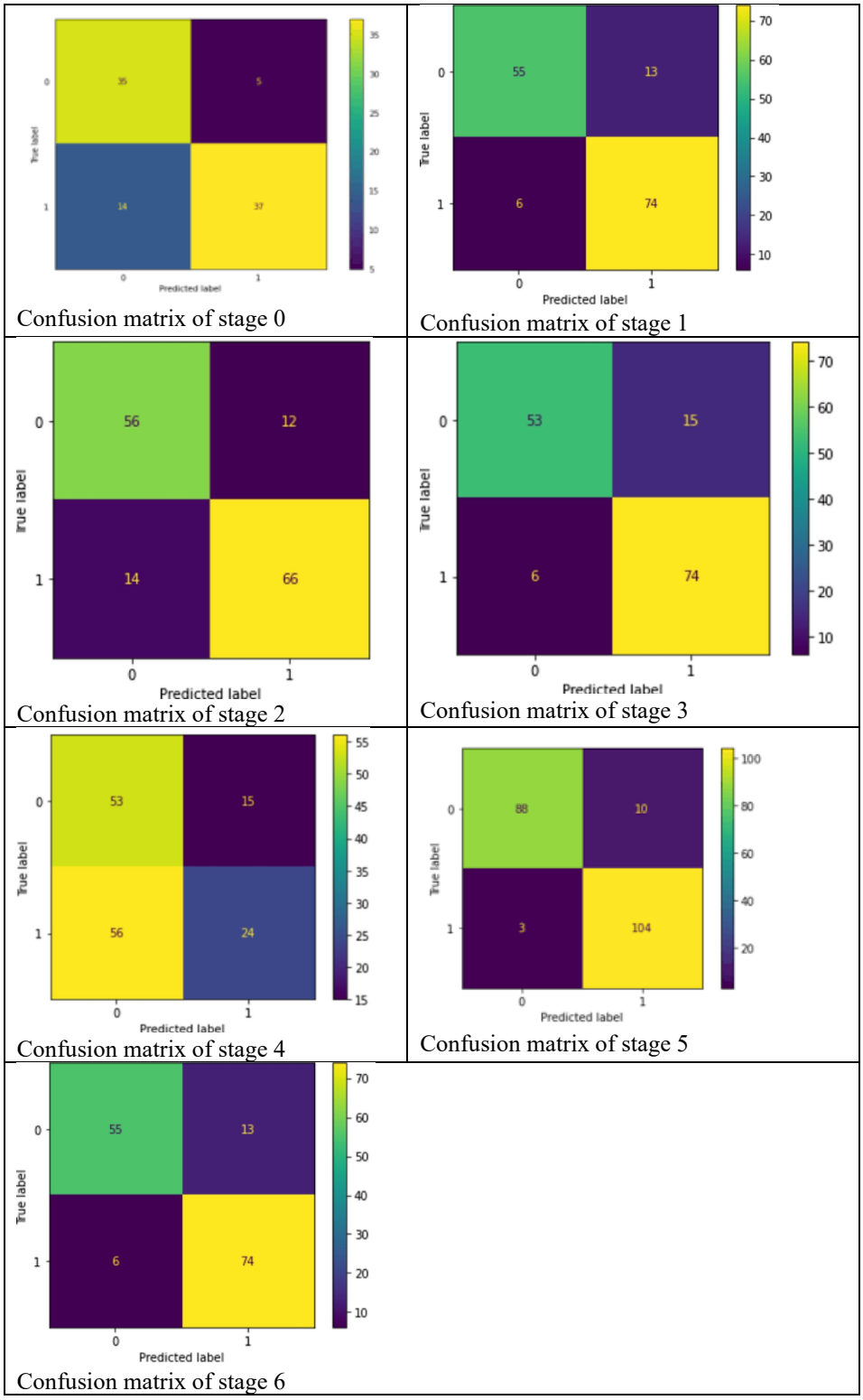

Figure 3: Confusion Matrix for Proposed MRI image dataset in stroke detection (a) stage 0 (b) stage 1, (c) stage 2, (d) stage 3, (e) stage 4, (f) stage 5, (g) stage 6

10. ROC curve based on various stages of stroke using proposed model:

Figure 4 displays ROC curve for suggested models. The ROC curve, where x-axis represents precision and y-axis represents recall, is an index that expresses the threshold and performance of binary classification prediction of stroke illness.

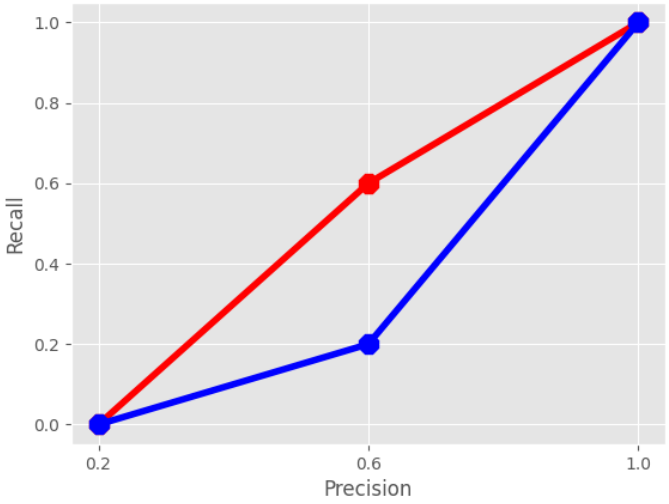

Figure-4 The ROC curve of the proposed stroke detection model

Traditionally, accuracy (Acc) is used to gauge the effectiveness of detection. The stroke datasets, however, showed an imbalance: there were more survival (n = 13,971) than non-survival (n = 1038) data. As a result, we employed three more metrics: positive predictive value (PPV), recall (Re), and precision (Pr). Re denotes probability of detecting survival, Re is probability of recognizing non-survival, PPV is probability that non-survival status was appropriately corrected. To assess performance of method, we employed four parameters: FP, FN, TP, TN. Correctly anticipated non-stroke rate is denoted by TN, and correctly predicted stroke rate is represented by TP. The inaccurately estimated stroke and non-stroke rates are denoted by the letters FP and FN.

Table-3 Comparative for various stages of stroke

Techniques	Stages of stroke	Training accuracy	Validation Accuracy	Recall	Precision	F1-score	Kappa coefficient
CNN	Stage 0	66	67	63	69	68	57
	Stage 1	68	70	67	72	71	61
	Stage 2	70	73	69	74	73	64
	Stage 3	72	76	71	77	76	67
	Stage 4	74	79	73	80	79	70
	Stage 5	79	81	76	82	82	72
	Stage 6	82	83	81	84	85	75
KNN	Stage 0	71	73	70	68	62	67
	Stage 1	73	75	75	73	65	71
	Stage 2	75	78	79	75	69	74
	Stage 3	77	81	82	78	72	77
	Stage 4	80	83	85	81	75	80
	Stage 5	82	87	87	86	78	82
	Stage 6	85	90	89	91	81	85
CBTC-GSwClA_DANSegNet	Stage 0	80	83	85	75	79	77
	Stage 1	84	86	87	79	83	81
	Stage 2	88	89	90	82	86	84
	Stage 3	91	92	93	87	88	87
	Stage 4	93	94	95	90	91	90
	Stage 5	95	96	97	93	94	92
	Stage 6	98	99	98	96	97	94

A comparison of the suggested and current methods for various stages of stroke is presented in Table 3 above. The Training accuracy, Validation Accuracy, Recall, Precision, and F1-score of proposed CE-LQCDFKA and the current CNN, KNN, have all been compared and contrasted. We employed two techniques to avoid overfitting: dropout and batch normalisation. Dropout employs weighting to minimise effects of specific hidden nodes, while batch normalisation minimises loss of feed-forward data in a way similar to suitable weighting on initialisation. The Re, Pr, PPV, Acc were evaluated as follows by eqn (12)

$$Re = TP/(TP + FN)$$
$$Pr = TN/(TN + FP)$$
$$PPV = TP/(TP + FP)$$
$$Acc = (TP + TN)/(TP + FN + FP + TN) \quad (12)$$

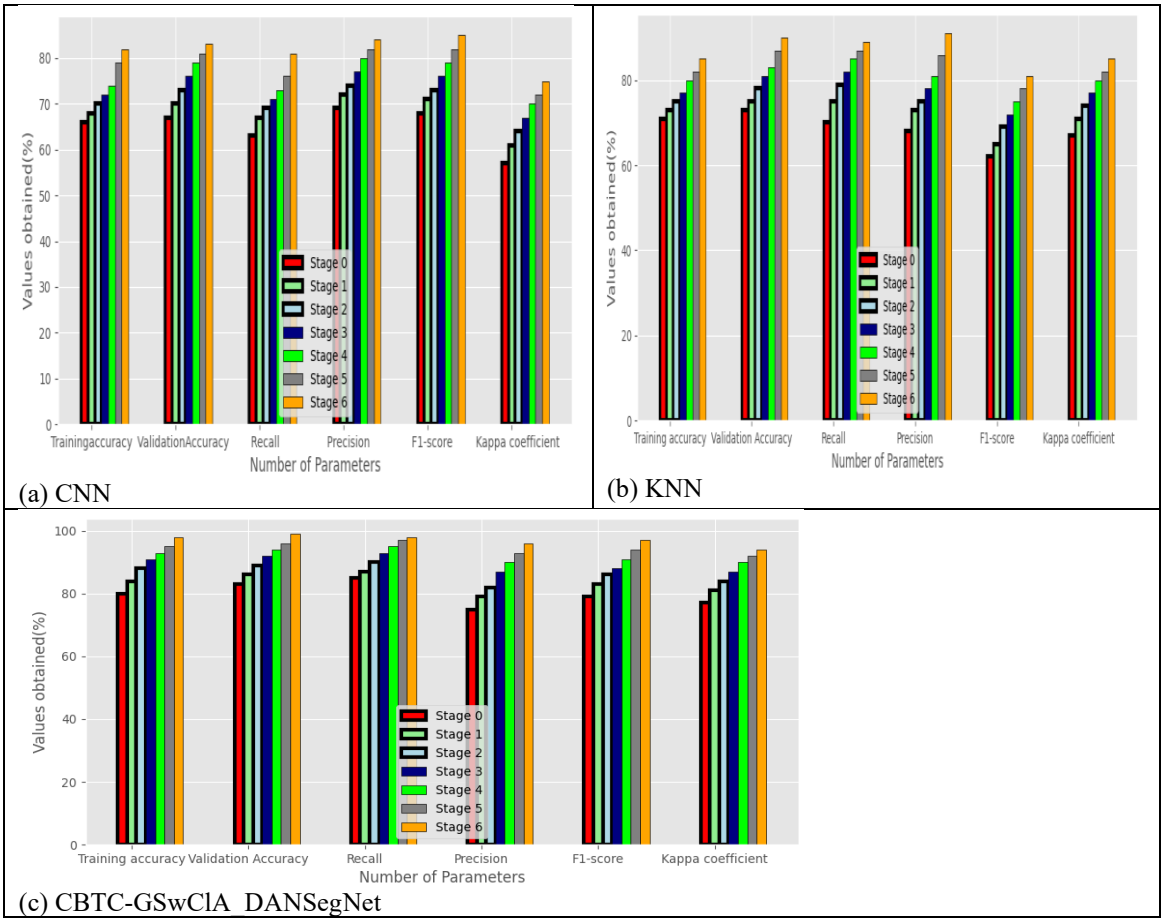

Figure-5 (a)- (c) Comparative for various stages of stroke (a) CNN, (b) KNN, (c) CBTC-GSwClA_DANSegNet

Figure 5(a)–(c) above illustrates the parametric analysis of the current various stages of stroke. The current CNN achieved 81% Recall, 84% Precision, 83% Validation accuracy, 82% Training accuracy, and a 85% F1-score, kappa co-efficient of 75% for stage 6; for stage 6 of stroke, the existing KNN achieved 89% Recall, 91% Precision, 90% Validation accuracy, 85% Training accuracy, and a 81% F1-score, kappa co-efficient of 85%; the proposed technique achieved 96% Precision, 99% Validation accuracy, 98% Training accuracy, and a 97% F1-score, recall of 98%, kappa co-efficient of 94% for stage 6 of stroke. The work employed T-1 weighted images from the brain MRI dataset. As a baseline, the model is trained again. During this phase, the network is not updated instead, its convolution layers are freeze. Only fully-connected layers' weights were trained in this model.

Model is trained for 4 epochs using multinomial logistic cost function, which allowed us to evaluate loss and error rate with a step size of 1e −3. To make sure method doesn't overfit on the training set, we set number of epochs to 4. Performance outside of sample is impacted by the model's memorisation of the provided tiny dataset. A 3∗3 convolution kernel is then called to predict on 6 feature layers with varying widths as well as depths in order to acquire classification, after many convolutional layers have been added. Next, the preselection box regression's predicted value is computed, final result is obtained with network loss.

Advantages and limitation: Using brain MRIs, the suggested classifier might potentially reliably classify different illness types. The tests in this study were limited to brain magnetic resonance imaging. Nevertheless, the suggested method might also yield precise results for MR scans of various body areas. The suggested model was deemed to be the most effective model for utilising MR images to identify multiple brain strokes after evaluating the performance and overall scores.

Future work might look into adding more datasets with different features, testing method on different diseases and imaging modalities, adding methods to deal with different image sizes and resolutions in order to overcome these limitations.

11. Conclusion and future scope:

Using an MRI brain image and a bio-inspired deep learning model, this research proposes a novel technique for stroke diagnosis that combines brain image segmentation with multi-classification. Here, MRI brain images are gathered as input, and the images have already undergone normalisation and noise reduction preprocessing. Next, using the genetic swarm clonal method (CBTC-GSwClA), the generated picture is segmented using traditional Boltzmann transfer convolution. The brain MRI regions with stroke prediction are visible in the segmented image, which will be identified using deep adversarial naïve SegNet architecture (DANSegNet). The several stroke classifications displayed in this categorised output range from stage 0 to 6. Variable size imaging data may not be appropriate for the suggested model since it uses fixed picture size and resolution. In terms of performance and

generalisation, the suggested model may be constrained by the small amount of data used for training. The suggested model has only been evaluated for class classification; additional testing as well as validation on multi-class classification are required to validate model's robustness. Encouraging findings suggest that general practitioners might utilise this automated multi-class classifier as a second opinion to help them make decisions faster. Future iterations of the suggested approach could include automated categorisation of various clinical states and disease kinds that are detected by hand from MRI data.

REFERENCES

1. Yousaf, F., Iqbal, S., Fatima, N., Kousar, T., & Rahim, M. S. M. (2023). Multi-class disease detection using deep learning and human brain medical imaging. Biomedical Signal Processing and Control, 85, 104875.
2. Rastogi, D., Johri, P., Tiwari, V., & Elngar, A. A. (2024). Multi-class classification of brain tumour magnetic resonance images using multi-branch network with inception block and five-fold cross validation deep learning framework. Biomedical Signal Processing and Control, 88, 105602.
3. Jaspin, K., & Selvan, S. (2023). Multiclass convolutional neural network based classification for the diagnosis of brain MRI images. Biomedical Signal Processing and Control, 82, 104542.
4. Srinivasan, S., Francis, D., Mathivanan, S. K., Rajadurai, H., Shivahare, B. D., & Shah, M. A. (2024). A hybrid deep CNN model for brain tumor image multi-classification. BMC Medical Imaging, 24(1), 21.
5. Prasad, R., & Shukla, P. K. (2023). Identification of Ischemic Stroke Origin Using Machine Learning Techniques. In Advances in Data-driven Computing and Intelligent Systems: Selected Papers from ADCIS 2022, Volume 2 (pp. 253-265). Singapore: Springer Nature Singapore.
6. Tufail, H., Ahad, A., Naqvi, M. H., Maqsood, R., & Pires, I. M. (2024). Classification of Vascular Dementia on magnetic resonance imaging using deep learning architectures. Intelligent Systems with Applications, 22, 200388.
7. Rumala, D. J., van Ooijen, P., Rachmadi, R. F., Sensusiati, A. D., & Purnama, I. K. E. (2023). Deep-Stacked Convolutional Neural Networks for Brain Abnormality Classification Based on MRI Images. Journal of Digital Imaging, 36(4), 1460-1479.
8. Bhagyalaxmi, K., Dwarakanath, B., & Reddy, P. V. P. (2024). Deep learning for multi-grade brain tumor detection and classification: a prospective survey. Multimedia Tools and Applications, 1-23.
9. Sundaram, M. S., Karthick, S., & Thiyagarajan, P. (2023, September). Hybrid Approaches for Intracerebral Hemorrhage Stroke Classification Using Deep Learning Techniques. In 2023 4th International Conference on Smart Electronics and Communication (ICOSEC) (pp. 885-890). IEEE.
10. Saha, P., Das, S. K., & Das, R. (2023). A Review on Machine Learning and Deep Learning Based Systems for the Diagnosis of Brain Cancer. SN Computer Science, 5(1), 28.
11. Solanki, S., Singh, U. P., Chouhan, S. S., & Jain, S. (2023). Brain tumor detection and classification using intelligence techniques: an overview. IEEE Access, 11, 12870-12886.
12. Nogay, H. S., & Adeli, H. (2024). Multiple classification of brain MRI autism spectrum disorder by age and gender using deep learning. Journal of Medical Systems, 48(1), 15.
13. Chen, S., Duan, J., Zhang, N., Qi, M., Li, J., Wang, H., ... & Qi, S. (2023). MSA-YOLOv5: Multi-scale attention-based YOLOv5 for automatic detection of acute ischemic stroke from multi-modality MRI images. Computers in Biology and Medicine, 165, 107471.
14. Devi, K. G., & Balasubramanian, K. (2024). Multivariate technique for the Prediction and Classification of Brain Tumor using deep shallow network. Applied Soft Computing, 111962.
15. Arafa, D. A., Moustafa, H. E. D., Ali, H. A., Ali-Eldin, A. M., & Saraya, S. F. (2024). A deep learning framework for early diagnosis of Alzheimer's disease on MRI images. Multimedia Tools and Applications, 83(2), 3767-3799.
16. Diwan, T., Gajbhiye, S. M., Goydani, P. R., Gannarpwar, V. R., Khandait, H. R., Tembhurne, J. V., & Sahare, P. (2024). Early detection of stroke disease using patients previous medical data instil with deep learning. Multimedia Tools and Applications, 1-29.
17. Diker, A., Elen, A., & Subasi, A. (2023). Brain stroke detection from computed tomography images using deep learning algorithms. In Applications of artificial intelligence in medical imaging (pp. 207-222). Academic Press.
18. Abujaber, A. A., Imam, Y., Albalkhi, I., Yaseen, S., Nashwan, A. J., & Akhtar, N. (2024). Utilizing machine learning to facilitate the early diagnosis of posterior circulation stroke. BMC neurology, 24(1), 156.
19. Yoon, C., Misra, S., Kim, K. J., Kim, C., & Kim, B. J. (2023). Collaborative multi-modal deep learning and radiomic features for classification of strokes within 6 h. Expert Systems with Applications, 228, 120473.
20. UmaMaheswaran, S. K., Ahmad, F., Hegde, R., Alwakeel, A. M., & Zahra, S. R. (2024). Enhanced non-contrast computed tomography images for early acute stroke detection using machine learning approach. Expert Systems with Applications, 240, 122559.
21. Aktar, M., Reyes, J., Tampieri, D., Rivaz, H., Xiao, Y., & Kersten-Oertel, M. (2023). Deep learning for collateral evaluation in ischemic stroke with imbalanced data. International Journal of Computer Assisted Radiology and Surgery, 18(4), 733-740.
22. Lin, S. Y., Chiang, P. L., Chen, M. H., Lee, M. Y., Lin, W. C., & Chen, Y. S. (2023). DGA3-Net: A parameter-efficient deep learning model for ASPECTS assessment for acute ischemic stroke using non-contrast computed tomography. NeuroImage: Clinical, 38, 103441.
23. Abbasi, H., Orouskhani, M., Asgari, S., & Zadeh, S. S. (2023). Automatic brain ischemic stroke segmentation with deep learning: A review. Neuroscience Informatics, 100145.

24. Tasci, B. (2023). Automated ischemic acute infarction detection using pre-trained CNN models' deep features. Biomedical Signal Processing and Control, 82, 104603.

25. Mishra, I., & Mohapatra, S. (2023). An enhanced approach for analyzing the performance of heart stroke prediction with machine learning techniques. International Journal of Information Technology, 15(6), 3257-3270.